www.gondwanags.org.in
Research Article

ISSN : 2455-1953
JGSR
Journal of Geosciences Research
Vol. 10, No.1, January, 2025, pp. 53-61

Geochemical Analysis of Paleocene-Eocene Sediments from Subathu Formation, Dehradun District, Uttarakhand: Implication for Provenance, Tectonic Setting and Paleoclimate

Shivaji P. Kokate[1], Shyam N. Mude[1]*, Ravindrasing G. Pardeshi[1]and Harshal N. Babar[2]

[1]*Department of Geology, Fergusson College (Autonomous), Pune-411004 (MS), India*
[2]*Department of Natural Resources and Environmental Studies, National Dong Hwa University, Hualien -9740, Taiwan*
*(*Corresponding Author, E-mail:shyam.mude@fergusson.edu)*

Abstract

The Palaeocene-Eocene Subathu Formation in the Nilkanth region near Rishikesh, Uttarakhand provides insights into the provenance, depositional environment, and tectonic setting prior to final India-Asia continent collision. Geochemical analysis of major oxides, trace elements, and rare earth elements from shale-dominated sedimentary rocks reveals a complex provenance. Discriminant function plots indicate the derivation of sediments from quartzose sedimentary sources, with minor input from mafic igneous sources. Trace element patterns suggest contributions from felsic igneous rocks, recycled sediments, and subduction-related components. The Chemical Index of Alteration (87.2* Avg.) indicates moderate weathering in the source area under semi-arid paleoclimatic conditions. Tectonic discrimination diagrams indicate that the deposition of sediments from Subathu Formation was occurred predominantly in an active continental margin setting. Rare earth element patterns exhibit varying degrees of fractionation, implying diverse sources ranging from mafic to felsic compositions. This multi-proxy geochemical study sheds light on the evolving paleoenvironmental conditions and sediment routing systems in the western Himalayan foreland basin leading up to the terminal India-Asia collision.

Keywords: Geochemistry, Subathu Formation, Provenance, Tectonic Setting, Paleoclimate, Depositional Environment, Himalaya

Introduction

Geochemical composition of clastic rocks has been widely used as a tool for determining the provenance, depositional environment, tectonic setting and weathering intensity (Fedo *et al.*, 1995; Bhatia, 1983; Suttner and Dutta, 1986; Pandey and Parcha, 2017; Pandey *et al*., 2023; Mude *et al.*, 2019, 2020; Talukdar *et al.,* 2022; Hakimi *et al.,* 2024). These parameters were designed based on how different elements react during the erosion and sedimentation stages. The variations in chemical composition do reflect and justify the sedimentary evolution and past geological processes affecting the clastic rocks. Hence, the correlation between the source area and the sedimentary basin can be determined.

Subathu Formation of the Palaeocene -Eocene age was first described by Medlicott in the year 1864. This formation represents the last marine transgression in the Himalayan foreland basin and is majorly outcropped at three locations which resemble as blocks: Nilkanth, Dharampur and Kalakot. This formation is mainly composed of fossiliferous limestones, shales, siltstones, and calcareous sandstones. The present study area lies in and around Nilkanth Temple Hill (30° 4′ 52.82″ N, 78° 20′ 52.64″ E to 30° 4′43. 15″ N, 78° 21′ 20.32″ E), which is 32 km form Rishikesh town towards east.

The objective of this study is to identify the source rock composition / provenance, tectonic setting, depositional environment and degree of weathering by using geochemical proxies such as major, trace and rare earth elements of clastic rocks belonging to the Lower-Middle Eocene Subathu Formation exposed in and around Nilkanth Temple Hill, Dehradun.

Geological Setting

The Sub-Himalayan region hosts a remarkable sequence of sedimentary rocks from the Palaeogene period, which provide a unique window into the tectonic evolution associated with the convergence of the Indian and Asian plates. This succession was deposited in a foreland basin that formed after the withdrawal of the Neo Tethys Sea, an ancient ocean that once separated these two continental masses (Kumar and Loyal, 2006)

The present sedimentary archive records distinct phases of the retreat of the Tethyan waters as the Indian and Asian plates converged, marking the transition from marine to continental sedimentation following the initial collisional contact. Consequently, these rock units serve as a valuable repository of information,

(Received : 07 October 2024 ; Revised Form Accepted : 20 December 2024)
https://doi.org/10.56153/g19088-024-0232-70

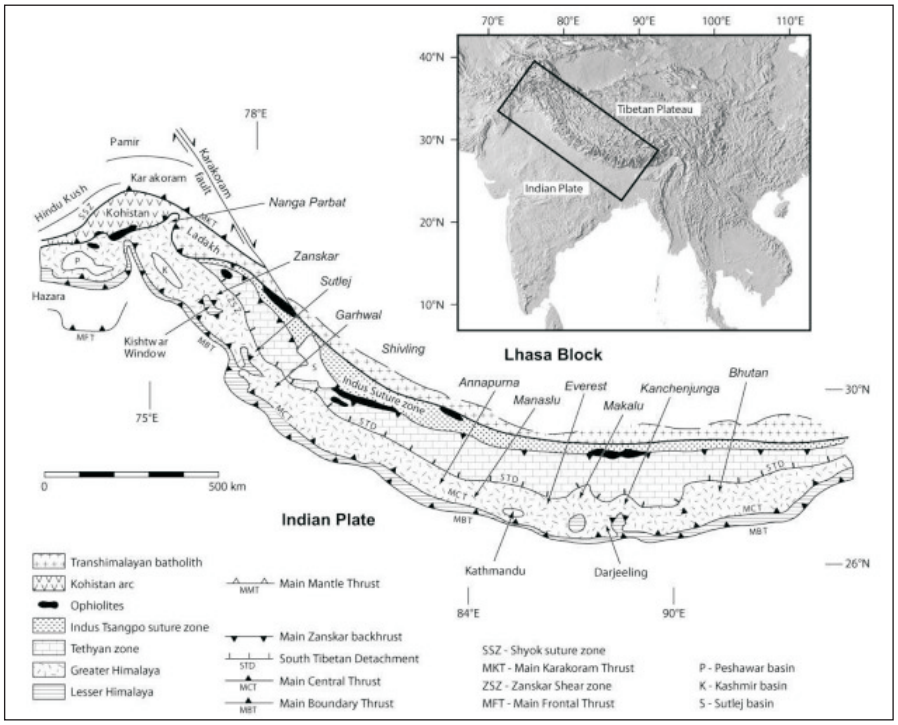

Fig.1. Map representing the geological setting of the Himalayas in which the Sub- Himalayan orogeny lies towards the south bounded by MCT and MBT (Searle *et al*., 2008)

offering insights into the pre-collisional, syn-collisional, and post-collisional stages of the closure of the Tethys Sea.

The Sub- Himalaya or Lesser Himalaya orogeny, also known as the Siwaliks, represents the southern front of the Himalayan range. It is bounded by the Main Frontal Thrust (MFT) in the south and the Main Boundary Thrust (MBT) in the north (Searle *et al.*, 2008; Fig.1).

The main formations from the Palaeogene period in the Sub-Himalayan region are the Subathu and Dagshai Formations, along with their equivalents (Kumar and Loyal, 2006). Exposures of these formations occur across a northwest-southeast trending belt. From the northwest, these Palaeogene Formations exposed in the Rajouri District of Jammu and Kashmir, in parts of Himachal Pradesh *viz.*, Dharampur, Solan and Sirmur, and further continuing towards the southeast, these formations were exposed in places like Lansdowne, Dogadda, and Rishikesh in Uttarakhand (Fig. 2).

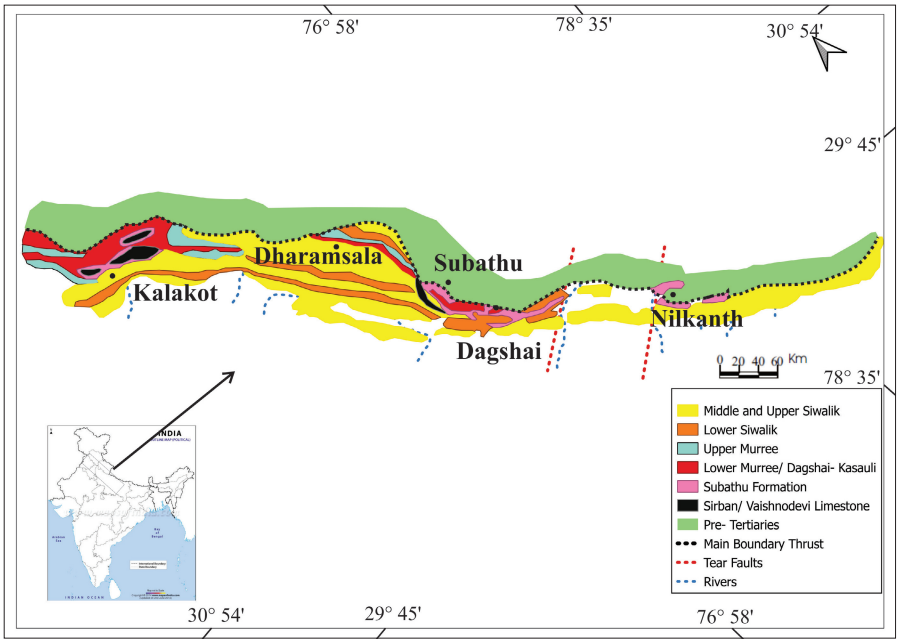

Fig.2. Section representing geographical distribution of Sub-Himalaya successions *viz.* Subathu, Dagshai, Kasauli and their equivalents (Karunakaran and Ranga Rao, 1976)

The sub-Himalayan sedimentary succession has been extensively studied through stratigraphic investigations by various researchers (Thakur, 1998, Jain *et al*., 2012; Todon, 2022; Valdiya, 1980) leading to the evolution of refined stratigraphic frameworks over time. Pioneering work of Medlicott (1864) established the rocks in to Subathus (lowermost), Nahuns, and Sivaliks (uppermost) units. Later, detailed investigations by Kumar and Loyal (2006), refined stratigraphy, subdividing sequence into distinct lithostratigraphic units. This framework widely adopted in contemporary geological studies (Table 1).

This subdivision comprises, in ascending order, the Subathu Formation, Dagshai Formation, Kasauli Formation, Murree Group, and the Siwalik Group. The stratigraphic nomenclature and interpretations have been subject to continuous refinement, reflecting the ongoing efforts to enhance the understanding of the complex tectonic and sedimentary history of the Sub-Himalayan belt through integrated field investigations, paleontological studies, and analytical techniques. The still evolving stratigraphic frameworks serve as a reference for ongoing research and provide a contextual basis for interpreting the geological processes and events that shaped the region.

Table 1: Lithostratigraphy of the Sub- Himalayan series for Subathu Formation (Kumar and Loyal, 2006)

Medlicott, 1864			Medlicott, 1876		Kumar and Loyal, 2006	
Sub-Himalayan Series	Sivaliks Nahuns		Sivaliks Nahuns		Siwalik Group	
	Subathus	Kasaolis	Sirmur Series	Kasaolis	Murree Group	Kasauli Formation
		Dugshais		Dugshais		Dagshai Formation
		Subathus		Subathus	Subathu Group	Subathu Formation
						Kakara Formation

Regional Geology

The regional geology around Rishikesh town is characterized by the presence of the Subathu Formation, a significant stratigraphic unit within the Sub-Himalayan Palaeogene succession (Kumar and Loyal, 2006). This formation is well-exposed in the area and comprises a sequence of alternating shales, limestones, and calcareous sandstones, deposited in a marine environment during the Late Palaeocene to Middle Eocene epochs (Garzanti *et al*., 1987). The Subathu Formation in the Rishikesh region is subdivided into three members: The Lower Subathu, characterized by dark grey to black shales with plant fossils and coal seams; the Middle Subathu, consisting of fossiliferous shales, siltstones, and limestones and the Upper Subathu, dominated by sandstones and shales (Mathur, 1980). These lithological variations reflect the gradual transition from a paralic to a fully marine depositional environment and subsequent shallowing of the basin. This formation overlies the Krol and Tal Formations in this area. The Subathu Formation in this area has been the subject of numerous studies, particularly for its rich fossil content, which has provided valuable insights into the paleoenvironmental conditions and paleobiogeographic affinities of the region during the Palaeogene period (Garzanti *et al*., 1987).

The present study area is situated around the Nilkanth Temple Hill, (30° 4′ 52.82″ N, 78° 20′ 52.64″ E) located east of Rishikesh town. The Subathu Formation is exceptionally well-exposed in road cuttings along the feeder road connecting Kothar village to Nilkanth Temple. This area offers an ideal location for geological investigation, as the Subathu Formation overlies the Tal Formation providing valuable insights into the stratigraphic relationships between these units. (Mathur, 1980). The succession is thrust against the rocks of the Almora/Garhwal Group. As a result of it the Subathu Formation is exposed at Nilkanth, the rest being cut off by the thrust.

Study Area

The fieldwork for the present study was meticulously conducted along the road connecting Kuthar village and Nilkanth Temple, where the Subathu Formation is well-exposed along the road cuttings. These outcrops provide an excellent opportunity to investigate the lithological variations and stratigraphic succession of the formation in the area.

A systematic sampling approach was adopted to ensure representative coverage of the exposed sequence. A total of twenty samples, comprising sandstones, shales, and limestones, were collected from these road-cut exposures along the traverse spanning an elevation range of 799 to 908 meters above sea level (Fig.3).

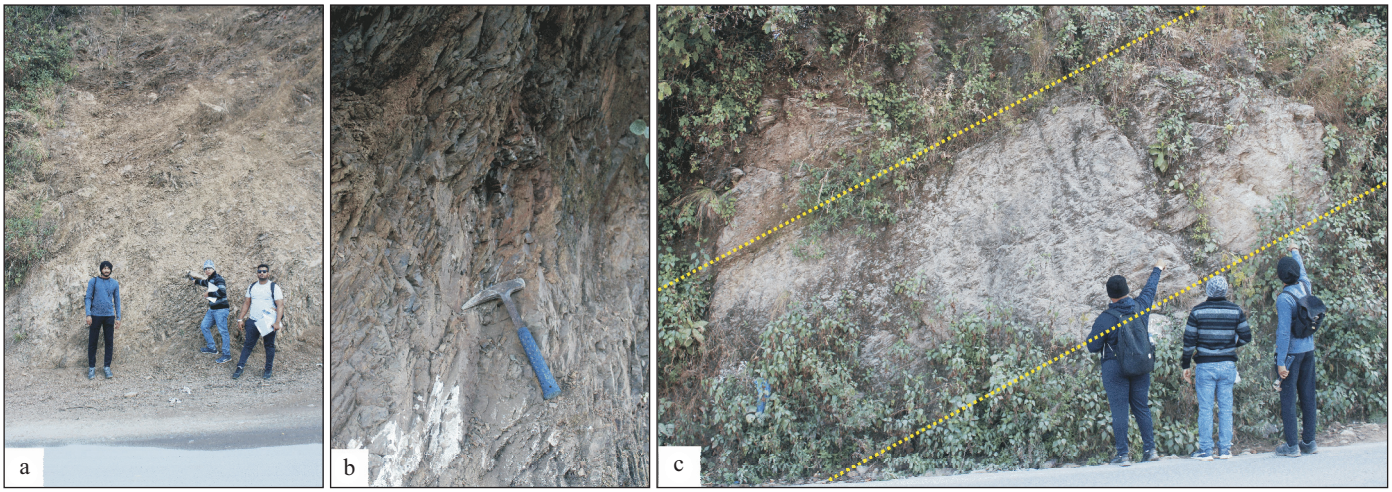

Fig. 3. Field photographs showing different locations from which the sediments of Subathu Formation were exposed around Nilkanth block; a) Outcrop showing exposed lithology as brown (Khaki) shale (Subathu Formation) which was exposed along the road cutting, road towards Nilkanth Temple; b) Fissile/ sharp-pointed brown shale exposure (Subathu Formation); c) Gently dipping bed, exposed lithology is limestone (Subathu Formation) along the traverse.

The sampling sites were carefully selected to encompass the entire observed stratigraphic thickness along the mountain trail, extending from the village of Kuthar to the parking area at the Nilkanth temple. The sampling locations were precisely marked and recorded using a global positioning system (GPS) device, enabling accurate spatial referencing and future cross-referencing. Furthermore, detailed field observations were documented, including lithological descriptions at each sampling site (Fig. 4).

The lithology represents the vertical lithological succession encountered along the studied section (Fig. 4). The basal part of the sequence is not exposed. The lithounits are dominated by alternating limestone and shale intervals, with a distinct yellow shale horizon in the middle part. Towards the top, thin brown shale and calcareous sandstone layers are present. The lithofacies associations and their ascending patterns suggest a transition from marine to marginal marine depositional conditions, with the yellow shale potentially representing a condensed interval or regional marker bed within the Middle Subathu Member of the formation.

Materials and Methods

Twenty rock samples were collected from the field area exposing the Subathu Formation. Out of these, ten clastic samples, predominantly shale, were selected for X-ray fluorescence (XRF) and Inductively Coupled Plasma Mass Spectrometry (ICP-MS) analyses. The selected samples were thorough washed with distilled water to remove potential contaminants and were subsequently powdered for analysis. Major oxide and trace element data were analyzed by using a Wavelength Dispersive X-Ray Fluorescence Sequential Spectrometer (WDXRF).

The XRF analysis was conducted to determine the major oxide concentrations (SiO_2, Al_2O_3, Fe_2O_3, TiO_2, CaO, MgO, MnO, Na_2O, K_2O, and P_2O_5), while the ICP-MS analysis was employed to quantify the trace elements (Sc, Co, Ni, Cu, Zn, Ga, Pb, Th, Rb, U, Sr, Y, Zr, Nb, Ba, Cr, V) and Rare Earth Elements (La, Ce, Pr, Nd, Sm, Eu, Gd, Tb, Dy, Ho, Er, Tm, Yb, Lu). These analyses were performed at the Wadia Institute of Himalayan Geology, Dehradun. The error in accuracy for major-minor oxides and trace elements analysis is < 5% and 12%, respectively with average error of 1.5%.

Rare earth elements (REE) were analyzed by Inductively Coupled Plasma Mass Spectrometer (ICP-MS, Perkin Elmer SCIEX ELAN DRC-e) using the open system rock digestion method. The error in accuracy of rare earth elements analysis ranges from 2 to 12% and precision varies from 1 to 8%. Wherever feasible, the obtained data were compared with the Post Archean Australian Shale (PAAS) reference values provided by Taylor and McLennan (1985). The Rare Earth Element (REE) concentrations were normalized to values reported by Taylor and McLennan (1985).

Results

The major oxide data reveals a predominantly silicic and aluminous composition across the samples. SiO_2 concentrations range from 47.46 to a remarkably high value of 81.03 wt%, significantly exceeding the Post-Archean Australian Shale (PAAS) and Upper Continental Crust (UCC) values of 62.3 and 66 wt %, respectively (Taylor and McLennan, 1985). Al_2O_3 exhibits a wide range, from 8.97 to 25.72 wt %, bracketing the PAAS (18.9 wt %) and UCC (15.2 wt %) values, suggesting varying degrees of alumina enrichment.

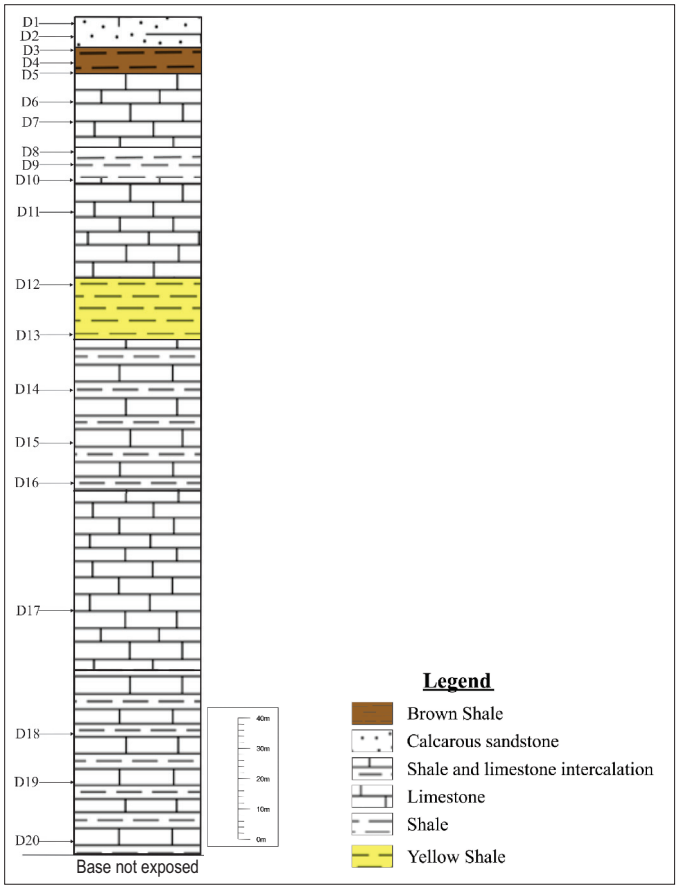

Fig.4. Image representing the lithology of the current study area with sample numbers (D1 to D20) of the Subathu Formation exposed in and around Nilkanth hill

The iron oxide (Fe_2O_3) concentrations display considerable variability, ranging from a depleted value of 2.15 to an enriched value of 10.21 wt %. These values are lower and higher, respectively, compared to the PAAS (7.23 wt %) and UCC (4.5wt %) averages, implying diverse iron enrichment processes across the samples. The alkali oxides (Na_2O and K_2O) also exhibit a wide range, indicating varying degrees of alkalinity and potential differences in source characteristics (Table 2).

The Rare Earth Element (REE) patterns generally exhibit enrichment in Light REEs (LREEs) compared to Heavy REEs (HREEs). La concentrations range from 13.665 ppm to 57.85 ppm, while Lu varies from 0.06 ppm to 0.42 ppm, deviating from the PAAS values of 34.714 ppm and 0.262 ppm, respectively (Table 2). Relative to PAAS, some samples are depleted in REEs (D3), while others are enriched (D12), indicating differences in source characteristics influencing the REE patterns across the samples.

Key indices for geochemical interpretation can be derived from these data (Table 2). The ratio of K_2O/Na_2O serves as an indicator of potassium alteration (Nesbitt and Young, 1982). Samples such as D16 (6.59) and D12 (5.67) exhibit elevated values, suggesting potassium enrichment, potentially due to weathering (McLennan, 1993). The Al_2O_3/TiO_2 ratio, used to evaluate aluminum-titanium fractionation, shows high values for D7 (42.7) and D15 (17.7), implying intense chemical weathering (Hayashi *et al.*, 1997). The SiO_2/Al_2O_3 ratio undergoes variations due to weathering processes and sediment recycling. In its unaltered state, the SiO_2/Al_2O_3 ratio typically ranges from approximately 3.0 for

Table 2: Geochemical composition results and elemental ratios of the samples

Elements	D1	D3	D5	D7	D12	D13	D15	D16	D18	D20	PAAS	UCC
Na_2O	0.7	0.57	0.89	3.35	0.66	0.85	0.48	0.44	0.53	0.54	1.2	3.9
MgO	2.55	2.45	2.74	0.34	2.55	2.14	2.57	3.15	3.49	3.06	2.2	2.2
Al_2O_3	21.18	16.96	15.93	8.97	25.72	15.62	13.84	16.02	17.47	13.54	18.9	15.2
SiO_2	54.46	61.61	60.33	81.03	47.46	62.63	55.97	60.53	54.66	58.77	62.3	66
P_2O_5	0.21	0.16	0.13	0.04	0.17	0.28	0.16	0.18	0.16	0.13	0.16	NA
K_2O	3.32	2.86	2.1	0.87	3.74	2.17	2.39	2.9	3.02	2.16	3.7	3.4
CaO	0.59	0.45	3.19	0.11	0.39	0.41	7.64	1.29	3.16	6.61	1.3	4.2
TiO_2	1.38	1.14	1.15	0.21	1.67	1.02	0.78	1.03	1.07	0.82	1	0.5
MnO	0.12	0.04	0.04	0.1	0.17	0.6	0.13	0.1	0.12	0.06	0.11	0.1
Fe_2O_3	8.89	9.23	7.38	2.15	10.21	8.85	5.89	7.88	8.7	5.84	7.23	4.5
L.O.I.	8.25	6.56	6.75	1.47	9.77	6.79	11.49	8.35	9.01	9.82		
SUM	101.65	102.03	100.63	98.64	102.51	101.36	101.34	101.87	101.39	101.35		
K_2O/Na_2O	4.74	5.02	2.36	0.26	5.67	2.55	4.98	6.59	5.7	4		
Al_2O_3/TiO_2	15.3	14.9	13.9	42.7	15.4	15.3	17.7	15.6	16.3	16.5	88.98	65.24
SiO_2/Al_2O_3	2.57	3.63	3.79	9.03	1.85	4.01	4.04	3.78	3.13	4.34	86.66	59.3
CIW	91.08	91.18	84.47	61.22	93.89	88.94	89.76	91.71	90.92	88.4	75.78	56.93
CIA	78.89	78.17	75.39	57.52	81.8	78.45	76.86	77.74	77.7	76.69		
PIA	102.03	101.61	107.03	105.57	101.64	101.91	114.29	102.88	106.38	112.57		
ICV	93.14	108.14	141.95	103.32	81.91	112.17	206.58	128.2	147.07	204.98		
Sc	19	16	14	3	20	16	13	15	14	12	16	
Co	23	20	21	5	32	16	15	28	26	16	23	17
Ni	126	115	70	15	111	76	85	140	118	86	55	44
Cu	51	43	50	8	45	28	32	35	28	40	50	25
Zn	129	121	123	30	135	113	90	118	113	94	85	71
Ga	21	18	14	4	26	16	11	15	17	9		
Pb	19	9	11	8	23	18	17	12	17	13	20	
Th	20	17	20	7	23	15	13	16	18	13	14.6	10.7
Rb	141	145	88	30	145	88	97	126	126	82	160	112
U	1.6	0.6	0.6	0.5	1.7	1	1.3	0.8	0.7	0	3.1	2.8
Sr	111	91	130	90	113	71	136	98	126	141	200	
Y	40	33	26	16	41	30	26	31	29	24		
Zr	311	238	345	165	338	255	191	208	234	213	210	71
Nb	27	22	23	4	27	17	16	21	22	18	1.9	25
Ba	345	256	246	164	338	454	226	254	267	186	650	
Cr	215	172	115	24	223	127	142	173	177	139	110	83
V	177	156	127	28	207	161	113	150	146	112	150	107
U/Th	0.08	0.03	0.03	0.07	0.07	0.07	0.1	0.05	0.04	0		
Ni/Co	5.48	5.75	3.33	3	3.47	4.75	5.67	5	4.54	5.38		
Sr/Cu	2.18	2.12	2.6	11.25	2.51	2.54	4.25	2.8	4.5	3.53		
Rb/Sr	1.27	1.59	0.68	0.33	1.28	1.24	0.71	1.29	1	0.58		
La	45.42	13.67	44.03	15.52	57.85	33.05	33.75	38.92	38.64	26.29	34.71	38.2
Ce	103.44	38.73	98.34	34.6	132.52	77.1	68.78	86.72	86.42	58.13	78.48	79.6
Pr	10.48	4.55	10.75	3.75	13.64	7.67	7.43	8.73	8.7	5.93	8.17	8.83
Nd	65.18	30.73	68.07	23.18	84.51	48.28	44.9	52.52	52.25	35.8	50.54	33.9
Sm	8.22	4.37	8.09	2.99	10.31	6.88	5.52	6.56	6.08	4.53	6.36	5.55
Eu	1.61	0.88	1.47	0.54	2.02	1.71	1.11	1.24	1.12	0.86	1.25	1.08
Gd	7	3.65	6.32	2.19	8.68	6.54	4.98	5.7	5.25	3.86	5.42	4.66
Tb	1.08	0.59	0.89	0.27	1.25	1.04	0.76	0.83	0.77	0.59	0.81	0.77
Dy	6.59	3.68	4.67	1.28	6.97	6.14	4.52	4.77	4.45	3.42	4.65	4.68
Ho	1.5	0.85	0.98	0.23	1.43	1.35	1	0.99	1	0.72	1	0.99
Er	3.67	2.01	2.4	0.57	3.4	3.17	2.48	2.31	2.41	1.69	2.41	2.85
Tm	0.58	0.33	0.36	0.08	0.51	0.51	0.39	0.36	0.38	0.26	0.38	0.41
Yb	2.94	1.71	1.87	0.44	2.54	2.52	1.96	1.75	1.9	1.28	1.89	2.82
Lu	0.42	0.24	0.26	0.06	0.35	0.35	0.27	0.24	0.26	0.18	0.26	0.43

basic rocks to around 5.0 for acidic rocks (Roser *et al*., 1996). The average SiO_2/Al_2O_3 ratio is 3.62, this suggests that the sediments are likely sourced from rocks with intermediate to acidic compositions, which are linked to chemical weathering processes.

Weathering and alteration indices, including the Chemical Index of Weathering (CIW), Chemical Index of Alteration (CIA), and Plagioclase Index of Alteration (PIA), provide insights into the extent of chemical weathering and mineral alteration (Fedo *et. al*., 1995). For instance, the high CIW value of D12 (93.89) and CIA value of PAAS (86.66) suggest intense weathering or alteration, while the lower CIA values of D7 (57.52) and UCC (59.3) indicate less weathered. Additionally, PIA values above 100, as observed in D15 (114.29) and D20 (112.57), signify plagioclase alteration (Fedo *et. al*., 1995).

The Index of Composition Variation (ICV) reflects the degree of compositional variation (Cox *et. al*., 1995). Higher ICV values, such as those observed in D15 (206.58) and D20 (204.98), suggest a recycled sedimentary source (Table 2).

Discussion

Provenance

The discriminant diagram, proposed by Roser and Korsch (1988), represents a widely adopted technique for provenance

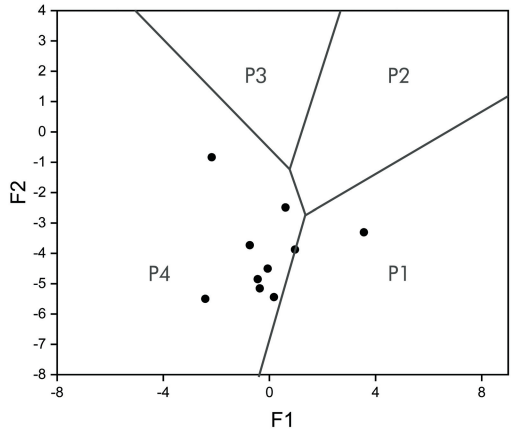

Fig.5. Provenance discrimination diagram for the collected samples of Subathu Formation, in and around Nilkanth area, Rishikesh (Roser and Korsch, 1988)

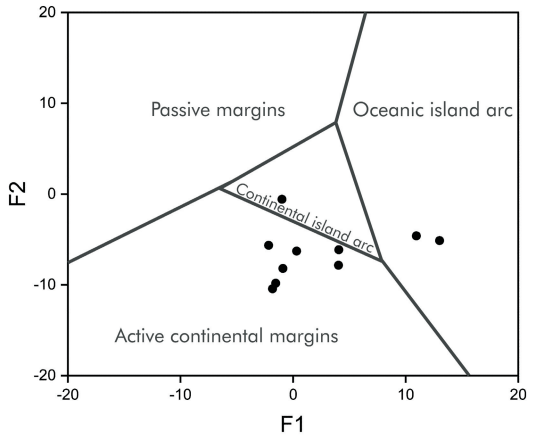

Fig.6. Discriminant function diagram plotted for the samples of Subathu Formation (*Fields derived after* Bhatia, 1983)

analysis. This approach utilizes discriminant functions derived from the concentrations of immobile and variable mobile major elements. The two functions are calculated using individual formulas and plotted against each other, providing a visual representation for interpreting provenance.

The key discriminating parameters employed in understanding provenance are TiO_2 and Al_2O_3. These elements are considered immobile and exhibit similar behaviour during fluvial transport and weathering processes.

The discriminant functions are defined as:

Function 1 (F1) = $(-1.733TiO_2 + 0.607Al_2O_3 + 0.76Fe_2O_3 - 1.5MgO + 0.616CaO + 0.509Na_2O - 1.224K_2O - 9.09)$

Function 2 (F2) = $(0.445TiO_2 + 0.07Al_2O_3 - 0.25Fe_2O_3 - 1.142MgO + 0.438CaO + 1.475Na_2O + 1.426K_2O - 6.86)$

According to Roser and Korsch (1988), samples falling within the P4 field of the discriminant diagram are indicative of a quartzose sedimentary provenance, while those in the P1 field suggest a mafic igneous provenance (Fig. 5).

Tectonic Setting

The chemical composition of sedimentary rocks is significantly influenced by the plate tectonic setting of their provenances. Different tectonic settings exhibit distinct geochemical signatures (Bhatia, 1983; Roser and Korsch, 1986). The tectonic setting can be deduced from a discriminant function analysis involving two functions proposed by Bhatia (1983).

Function 1 (F1) = $(-0.0447 \times SiO_2) + (-0.972 \times TiO_2) + (0.008 \times Al_2O_3) + (-0.267 \times Fe_2O_3) + (0.208 \times FeO) + (-3.082 \times MnO) + (0.140 \times MgO) + (0.195 \times CaO) + (0.719 \times Na_2O) + (-0.032 \times K_2O) + (7.510 \times P_2O_5)$

Function 2 (F2) = $(-0.421 \times SiO_2) + (1.988 \times TiO_2) + (-0.526 \times Al_2O_3) + (-0.551 \times Fe_2O_3) + (-1.610 \times FeO) + (2.720 \times MnO) + (0.881 \times MgO) + (-0.907 \times CaO) + (-0.117 \times Na_2O) + (-1.840 \times K_2O) + (7.244 \times P_2O_5)$

The tectonic discrimination diagram based on these functions suggests that the sediments of the Subathu Formation were derived from parent rocks formed in three distinct tectonic settings: Predominantly in an active continental margin, oceanic island arc, and continental island arc (Fig. 6).

This mixed signature reflects the complex paleogeography that existed prior to the final continental collision between India and Eurasia in the early Cenozoic.

Paleoclimate

The paleoclimatic conditions during the deposition of the Subathu Formation have been inferred from bivariant plots (SiO_2 vs $Al_2O_3+K_2O+Na_2O$) (*After* Suttner and Dutta, 1986; Fig.7).

This plot reveals semi-arid climate conditions, reflecting the climatic regimes during the sediments deposition. These interpretations influence sediment composition and depositional processes.

Chemical Classification of Sedimentary Rocks

Differentiation between quartz and feldspar rich sands can be achieved by considering the SiO_2/Al_2O_3 ratios (Herron 1988). Bivariant plots [(Log SiO_2/Al_2O_3) versus (Fe_2O_3/K_2O)] (Fig. 8) were plotted against each other which showed that the samples range fall under the region of shale, wacke and one sample falls under the field of lithic arenite.

Chemical Index of Alteration (CIA)

To understand the degree of chemical weathering, an index of

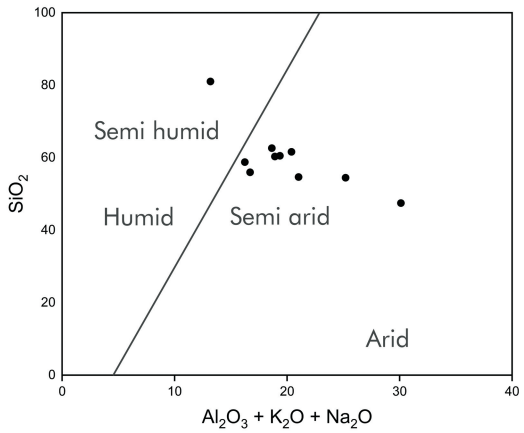

Fig.7. Bivariant plot for understanding the paleoclimatic conditions during the deposition (Fields derived *after* Suttner and Datta, 1986)

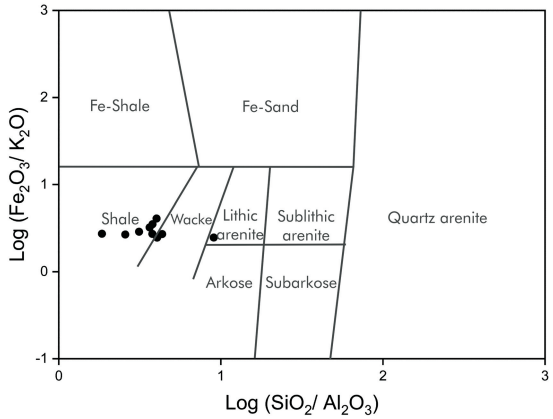

Fig.8. Bivariant plot for understanding the rock type classification with the help of chemical composition (*Fields derived after* Herron, 1988)

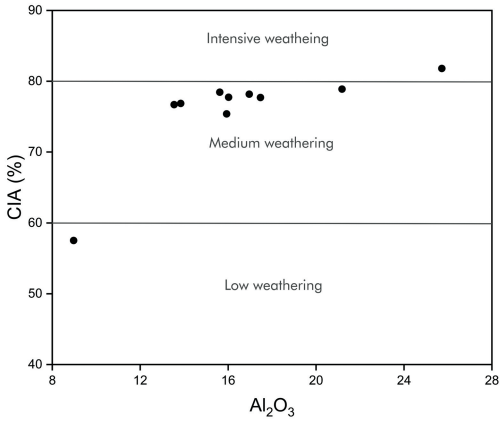

Fig.9. Bivariant plot plotted for the samples to understand the degree of chemical weathering (Nesbitt and Young, 1982)

chemical alteration (CIA) was proposed by Nesbitt and Young, 1982. CIA: [Al_2O_3/ (Al_2O_3 + CaO^* + Na_2O +K_2O)] x 100. Here Cao*(Cao* from silicates only) is converted into silicate fraction of the rock. The calculated CIA values are plotted against Al_2O_3 to understand the degree of chemical weathering (Nesbitt and Young, 1982; Fig. 9). Majority values fall into medium weathering except two falling in low weathering and intensive weathering, respectively indicating the early stages of depositions of these sediments.

Trace Element Geochemistry

The trace element distribution patterns for the analysed samples (D1, D3, D5, D7, D12, D13, D15, D16, D18, D20) exhibit distinct variations relative to the Post-Archean Australian Shale (PAAS) reference composition (Taylor and McLennan, 1985). The D1, D3, and D5 samples display enrichment in large ion lithophile elements (LILE: Rb, Ba, Sr) and depletion in high field strength elements (HFSE: Nb, Zr, Y) (Fig. 10), suggesting derivation from a more felsic source and input from arc-related magmatic sources (McLennan *et al.,* 1990). In contrast, the D7, D12, and D13 samples show relatively flat patterns with minimal fractionation between LILE and HFSE, indicative of a less evolved, mafic to intermediate source composition. The D15, D16, D18, and D20 samples exhibit pronounced negative Nb and Ti anomalies, potentially reflecting contributions from a subduction related source. Overall, the diverse trace element signatures imply that the analysed samples have been derived from multiple sources with varying degrees of crustal recycling and input from different tectonic settings, highlighting the complex provenance history of the studied sedimentary units (Taylor and McLennan, 1985; Bhatia 1983).

The normalized pattern reveals distinct trace element distributions among the analysed samples (D1- D20) when normalized to the Upper Continental Crust (UCC) composition (Fig. 11). The D7, D12, and D13 samples exhibit patterns that closely mirror the UCC, suggesting derivation from an average upper crustal source with minimal fractionation. In contrast, the D1, D3, and D5 samples display pronounced enrichment in LILE (Rb, Ba, Sr) and depletion in HFSE (Nb, Zr, Y) relative to the UCC, indicating derivation from a more evolved, felsic source or contributions from arc-related magmatic components. The D15, D16, D18, and D20 samples show distinct negative anomalies for Nb and Ti, which can be attributed to the incorporation of subduction-related components and the recycling of older sedimentary material depleted in these elements. The diverse trace element signatures observed across the samples, ranging from UCC-like patterns to those with substantial LILE enrichment and HFSE depletion, suggest a complex provenance involving contributions from various sources, including average upper continental crust, felsic igneous rocks, and recycled sedimentary components (McLennan *et al.*, 1990; Taylor and McLennan,1985).

The transition metal elements, such as Ni, Cu, Zn, and Co, exhibit substantial variations in their concentrations. For instance, Ni ranges from 15 ppm to 140 ppm, while Cu varies from 8 ppm to 51 ppm, both significantly deviating from the PAAS values of 55 ppm and 50 ppm, respectively (Table 2). These variations suggest diverse geochemical processes and the sources contributing to the enrichment of these elements across the samples.

The Large Ion Lithophile Elements (LILEs) and High Field Strength Elements (HFSEs) also display considerable variability. Rb concentrations range from 30 ppm to 145 ppm, compared to the PAAS value of 160 ppm. Ba varies from 164 ppm to 454 ppm, while the PAAS value is 650 ppm. Similarly, Zr ranges from 165 ppm to 345 ppm D5, and Nb varies from 4 ppm 7 to 27 ppm, contrasting with the PAAS values of 210 ppm and 1.9 ppm, respectively (Table 2).

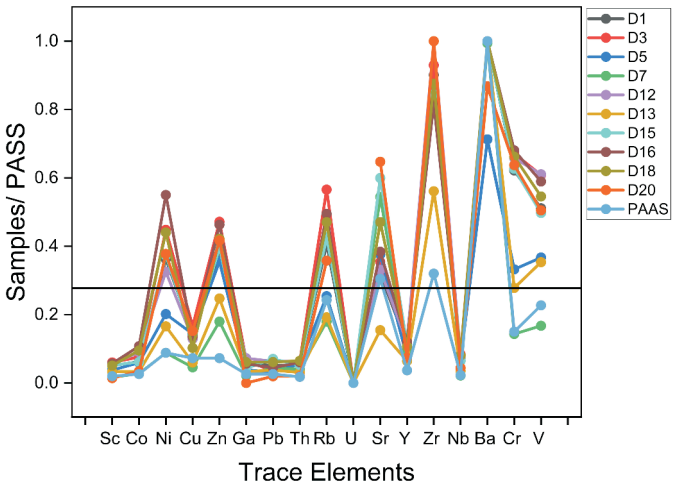

Fig.10. PAAS normalized trace elements spider diagram for the samples (*Normalization values after* Taylor and McLennan, 1985)

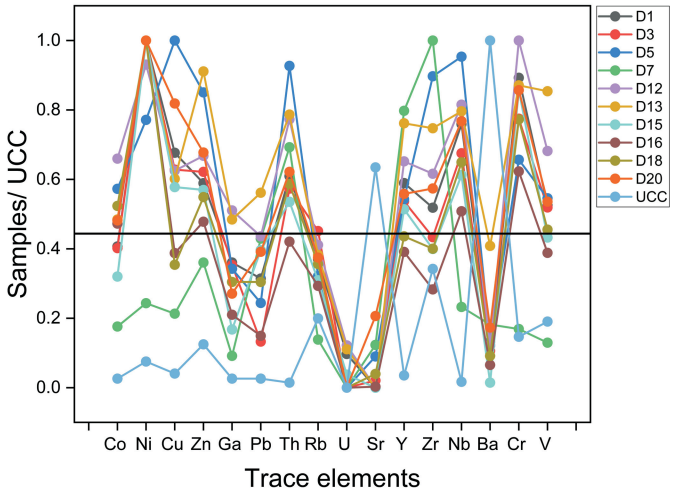

Fig.11. UCC normalized trace elements spider diagram for the samples (*Normalization values after* Taylor and McLennan, 1985)

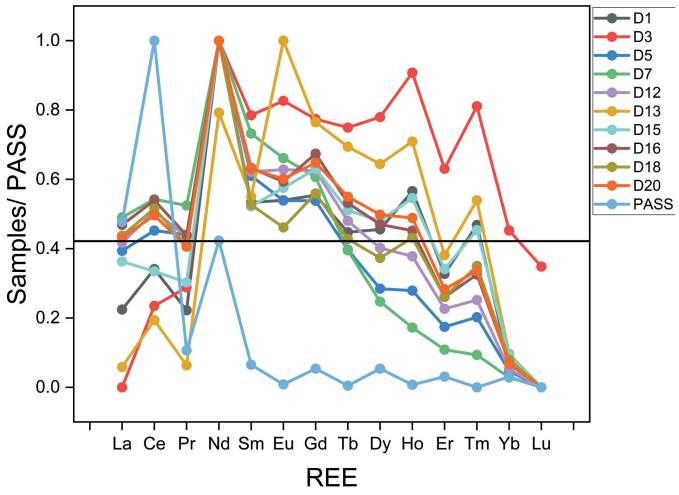

Fig.12. PAAS normalized against rare earth elements spider diagram for the samples (*Normalization values after* Taylor and McLennan, 1985).

These variations in LILE and HFSE concentrations suggest different degrees of fractionation or source characteristics influencing their distribution across the samples.

Rare Earth Geochemistry

The rare earth element patterns are exhibited by the analysed samples D1 to D20 (Fig. 12) display substantial variability when normalized to the Post-Archean Australian Shale (PASS) reference composition. The D1 sample shows a distinct pattern with a pronounced negative Eu anomaly, suggesting plagioclase fractionation and contributions from a source with residual plagioclase. The D3, D5, and D7 samples exhibit relatively flat REE patterns with slight light rare earth element (LREE) enrichment, indicative of minimal fractionation and derivation from a less evolved, mafic to intermediate source. In contrast, the D12, D13, D15, D18, and D20 samples display varying degrees of LREE enrichment relative to heavy rare earth elements (HREE), imply contributions from more evolved felsic sources. Notably, the D16 and D18 samples exhibit distinct negative Ce anomalies, which could be attributed to oxidizing conditions during sediment deposition and diagenesis which reflecting changes in redox conditions and input from different sources. The diverse REE signatures observed across the samples suggest contributions from multiple sources ranging from mafic to felsic compositions and involving different tectonic settings.

Conclusions

The detailed geochemical study of the Palaeocene Eocene Subathu Formation sedimentary rocks from the Nilkanth region near Rishikesh sheds light on their complex provenance history and paleoenvironmental conditions. Geochemical data indicate that the Subathu Formation received sediments from the northern passive margin. Provenance discrimination diagrams suggest that the sediments were mainly derived from quartzose sedimentary sources. This type of provenance is consistent with early rifting and erosion during the initial stages of the India-Asia collision. The geochemical data imply the recycling of older sedimentary material, as well as inputs from subduction-related and evolved felsic sources. The trace and rare earth elements pattern distribution pattern corroborate the complex provenance. Some sample exhibit characteristics typical of upper continental crust. Others display enrichments or depletions indicative of specific tectonic environments and fractionation processes. According to the chemical composition, the sediments from the Subathu Formation are classified as shale, wacke, and lithic arenite. The deposition occurred under semi-arid climatic conditions, and the tectonic setting through geochemical data is consistent with an active continental margin during that time. This study provides new geochemical insights into the paleoenvironmental and basin evolution of the western Himalayan foreland basin prior to final suturing along the Indus-Tsangpo Suture Zone.

Authors' Contributions

SPK: Conceptualization, Investigation, Writing-Original Draft. **SNM:** Visualization, Supervision, Investigation, Writing-Reviewing and Editing. **RGP:** Supervision, Writing-Reviewing and Editing. **HNB:** Data Collection, Formal Analysis, Writing - Original Draft.

Conflict of Interest

Authors declare that they have no conflict of interests.

Acknowledgements

The authors are thankful to Rahul Oswal, Aniket Choudhary, Mritunjay Vichare, Abhilash Sen, Ipsita Roy, Dinesh Mahajan and Manish Mahire for their support during the field works. The authors are thankful to Wadia Institute of Himalayan Geology, Dehradun for providing XRF and ICP-MS data of the samples. The authors are also thankful to Principal, Fergusson College, Pune and Head, Department of Geology, Fergusson College, Pune for their constant support and encouragement.

References

Bhatia, M.R. (1983). Plate tectonics and geochemical composition of sandstones. Jour. Geol., v. 91, pp. 611-627.

Cox, R., Lowe, D.R. and Cullers, R.L. (1995). The influence of sediment recycling and basement composition on evolution of mudrock chemistry in the southwestern United States. GCA, v. 59(14), pp. 2919-2940.

Fedo, C.M., Eriksson, K.A. and Krogstad, E.J. (1995). Geochemistry of shales from the Archean (~3.0 Ga) Buhwa Greenstone Belt, Zimbabwe: Implications for provenance and source-area weathering. Geochim. Cosmochim. Acta, v. 60, pp. 1751-1763.

Garzanti, E., Baud, A. and Mascle, G. (1987). Sedimentary record of the northward flight of India and its collision with Eurasia (Ladakh Himalaya, India). Geodin. Acta, v. 1(4-5), pp. 297-312.

Hakimi, M. H., Kumar, A., Alqubalee, A. M., Singh, A. K., Almobarky, M., Rahim, A. and Naseem, W. (2024). Mineralogy and Geochemistry of the Paleocene–Eocene Palana Formation in Western Rajasthan, India: Insights for Sedimentary Paleoenvironmental Conditions and Volcanic Activity. Minerals, v. 14(2), pp.126.

Hayashi, K.I., Fujisawa, H., Holland, H. D. and Ohmoto, H. (1997). Geochemistry of~ 1.9 Ga sedimentary rocks from northeastern Labrador, Canada. Geochim. Cosmochim. Acta, v. 61(19), pp. 4115-4137.

Herron, M.M., (1988). Geochemical classification of terrigenous sands and shales from core or log data. Jour. Sediment. Petrol., v. 58, pp. 820-829.

Jain, A.K., Ahmad, T., Singh, S., Ghosh, S.K., Patel, R.C., Kumar, Rohatash and Bhargava, O.N. (2012). Evolution of the Himalaya. Proc. Indian Natl. Sci. Acad., v. 78, pp. 259-275.

Karunakaran, C. and Rangarao, A. (1976). Status of exploration for hydrocarbons in the Himalayan region - Contributions to stratigraphy and structure. Geol. Surv. India Misc. Publ., v. 41, pp. 1-66.

Kumar, K. and Loyal, R.S. (2006). Excursion guide on sub-Himalayan Palaeogene succession of Shimla Hills (Subathu–Dagshai–Kasauli formations in Stratotype Area, Solan District, Himachal Pradesh). Unpublished, Wadia Institute of Himalayan Geology, Dehradun, 61p.

Mathur, N.S. (1980). Biostratigraphical aspects of the Subathu Formation, Kumaun Himalaya. Rec. Res. Geol., v. 5, Hindustan Publ. Corp., Delhi, pp. 96-112.

McLennan, S.M. (1993). Weathering and global denudation. Jour. Geol., v. 101, pp. 295-303.

McLennan, S.M., Taylor, S.R., McCulloch, M.T. and Maynard, J.B. (1990). Geochemical and Nd-Sr isotopic composition of deep-sea turbidites: Crustal evolution and plate tectonic associations. Geochim. Cosmochim. Acta, v. 54, pp. 2015-2050.

Medlicott, H.B. (1864). On the geological structure and relations of the southern portion of the Himalayan range between the rivers Ganges and Ravee. Mem. Geol. Surv. India, v. 3, pp. 1-206.

Medlicott, H.B. (1876). Notes upon the Sub Himalayan Series in the Jammu Hills. Rec. Surv. India, v. 9(2), pp. 49-57.

Mude, S.N., Parcha, S.K., Pandey, S. and Madane, S.B. (2019). Geochemistry, provenance, compositional maturity of Mastani lake sediments, India. Jour. Geosci. Res., v. 4(2), pp. 143-154.

Mude, S.N., Yawale, S. and Choudhari, V. (2020). Sedimentological and geochemical characterization of Manaveli and Cuddalore Formations, Puducherry Basin, India. Jour. Indian Assoc. Sedimentol., v. 37, pp. 115-130.

Nesbitt, H. and Young, G.M. (1982). Early Proterozoic climates and plate motions inferred from major element chemistry of lutites. Nature, v. 299(5885), pp. 715-717.

Pandey, S. and Parcha, S.K. (2017). Provenance, tectonic setting and source-area weathering of the Lower Cambrian sediments of the Parahio valley in the Spiti basin, India. Jour. Earth Syst. Sci., v. 126, pp. 1-16.

Pandey, S., Jalal, P., Parcha, S.K. and Sehgal, R.K. (2023). Geochemical characterization of the Middle Cambrian sandstones from Spiti Basin, India: Implications for paleoenvironment, provenance, and tectonic setting. Arab. Jour. Geosci., v. 16(1), p. 47.

Roser, B.P. and Korsch, R.J. (1986). Determination of tectonic setting of sandstone–mudstone suites using SiO2 content and K2O/Na2O ratio. Jour. Geol., v. 94, pp. 635-650.

Roser, B.P. and Korsch, R.J. (1988). Provenance signature of sandstone–mudstone suite determined using discriminant function analysis of major element data. Chem. Geol., v. 67, pp. 119-139.

Roser, B.P., Cooper, R.A., Nathan, S. and Tulloch, A.J. (1996). Reconnaissance sandstone geochemistry, provenance, and tectonic setting of the lower Paleozoic terranes of the West Coast and Nelson, New Zealand. NewZealand Jour. Geol. Geophys., v. 39(1), pp. 1-16.

Searle, M.P., Law, R.D., Godin, L., Larson, K.P., Streule, M.J., Cottle, J.M. and Jessup, M.J. (2008). Defining the Himalayan main central thrust in Nepal. Jour. Geol. Soc., v. 165(2), pp. 523-534.

Suttner, L.J. and Dutta, P.K. (1986). Alluvial sandstone composition and paleoclimate, I. Framework mineralogy. Jour. Sediment. Petrol., v. 56, pp. 329-345.

Talukdar, R., Kothyari, G.C., Pathak, M. and Pant, C.C. (2022). Geochemistry of the Kali River terrace sediments in Central Himalaya, India: Implication on nature of provenance in the known tectonic environment. Environ. Challeng., v. 9, pp. 100609.

Tandon, S.K. (2022). The Himalayan foreland basin-stratigraphic records of continent-to-continent collisional processes. Geol. Soc. India, pp. 1015-1015.

Taylor, S.R. and McLennan, S.M. (1985). The Continental Crust: Its Composition and Evolution. Blackwell, Oxford.

Thakur, V.C. (1998). Structure of the Chamba nappe and position of the Main Central Thrust in Kashmir Himalaya. Jour. Asian Earth Sci., v. 16(2-3), pp. 269-282.

Thakur, V.C. (2013). Active tectonics of Himalayan frontal fault system. Intl. Jour. Earth Sci., v.102, pp. 1791-1810.

Valdiya, K.S. (1980). Geology of Kumaun Lesser Himalaya. Wadia Institute of Himalayan Geology, Dehradun.